



Zhou, R., Han, Y., Cao, J., Li, M., Jin, G., Du, Y., ... Su, B. (2018). Enhanced Osseointegration of Hierarchically Structured Ti Implant with Electrically Bioactive SnO₂-TiO₂ Bilayered Surface. *ACS Applied Materials and Interfaces*, 10(36), 30191-30200. <https://doi.org/10.1021/acsami.8b10928>

Peer reviewed version

Link to published version (if available):
[10.1021/acsami.8b10928](https://doi.org/10.1021/acsami.8b10928)

[Link to publication record in Explore Bristol Research](#)
PDF-document

This is the author accepted manuscript (AAM). The final published version (version of record) is available online via ACS at <https://pubs.acs.org/doi/10.1021/acsami.8b10928>. Please refer to any applicable terms of use of the publisher.

University of Bristol - Explore Bristol Research

General rights

This document is made available in accordance with publisher policies. Please cite only the published version using the reference above. Full terms of use are available:
<http://www.bristol.ac.uk/pure/about/ebr-terms>

Enhanced osseointegration of hierarchically structured Ti implant with electrically bioactive SnO₂-TiO₂ bi-layered surface

Rui Zhou, Yong Han, Jianyun Cao, Ming Li, Guorui Jin, Yuzhou Du, Haoteng Luo, Yongchao Yang, Lizhai Zhang, and Bo Su

ACS Appl. Mater. Interfaces, **Just Accepted Manuscript** • DOI: 10.1021/acsami.8b10928 • Publication Date (Web): 21 Aug 2018

Downloaded from <http://pubs.acs.org> on August 22, 2018

Just Accepted

“Just Accepted” manuscripts have been peer-reviewed and accepted for publication. They are posted online prior to technical editing, formatting for publication and author proofing. The American Chemical Society provides “Just Accepted” as a service to the research community to expedite the dissemination of scientific material as soon as possible after acceptance. “Just Accepted” manuscripts appear in full in PDF format accompanied by an HTML abstract. “Just Accepted” manuscripts have been fully peer reviewed, but should not be considered the official version of record. They are citable by the Digital Object Identifier (DOI®). “Just Accepted” is an optional service offered to authors. Therefore, the “Just Accepted” Web site may not include all articles that will be published in the journal. After a manuscript is technically edited and formatted, it will be removed from the “Just Accepted” Web site and published as an ASAP article. Note that technical editing may introduce minor changes to the manuscript text and/or graphics which could affect content, and all legal disclaimers and ethical guidelines that apply to the journal pertain. ACS cannot be held responsible for errors or consequences arising from the use of information contained in these “Just Accepted” manuscripts.



1
2
3
4 Enhanced osseointegration of hierarchically structured Ti implant with
5
6 electrically bioactive SnO₂-TiO₂ bi-layered surface
7

8
9 *Rui Zhou*^{†‡}, *Yong Han*^{*†}, *Jianyun Cao*[⊥], *Ming Li*[⊤], *Guorui Jin*[¶], *Yuzhou Du*[§], *Haoteng Luo*[†],
10
11 *Yongchao Yang*[†], *Lizhai Zhang*[†], *Bo Su*^{*‡}
12
13

14 [†] State Key Laboratory for Mechanical Behavior of Materials, Xi'an Jiaotong University, Xi'an
15
16 710049, P.R. China
17
18

19 [‡] Bristol Dental School, University of Bristol, Bristol BS1 2LY, UK
20
21

22 [⊥] School of Materials, University of Manchester, Manchester M13 9PL, UK
23
24

25 [⊤] Honghui Hospital, Xi'an Jiaotong University College of Medicine, Xi'an 710054, P.R. China
26
27

28 [¶] Bioinspired Engineering and Biomechanics Center, Xi'an Jiaotong University, Xi'an 710049,
29
30 P.R. China
31

32 [§] School of Materials Science and Engineering, Xi'an University of Technology, Xi'an 710048,
33
34 P.R. China
35
36
37
38
39

40 **KEYWORDS:** Hierarchical structure, Electrical bioactivity, SnO₂-TiO₂, Ti implant,
41
42 osseointegration.
43
44
45
46
47

48 **ABSTRACT:** The poor osseointegration of Ti implant significantly compromise its application
49
50 in load-bearing bone repair and replacement. Electrically bioactive coating inspired from
51
52 heterojunction on Ti implant can benefit osseointegration but cannot avoid the stress shielding
53
54 effect between bone and implant. To resolve this conflict, hierarchically structured Ti implant
55
56
57
58
59
60

1
2
3
4 with electrically bioactive SnO₂-TiO₂ bi-layered surface has been developed to enhance
5
6 osseointegration. Benefiting from the electric cue offered by the built-in electrical field of
7
8 SnO₂-TiO₂ heterojunction and the topographic cue provided by the hierarchical surface structure
9
10 to bone regeneration, the osteoblastic function of basic multicellular units (BMUs) around the
11
12 implant is significantly improved. Because the individual TiO₂ or SnO₂ coating with uniform
13
14 surface exhibits no electrical bioactivity, the effects of electric and topographic cues to
15
16 osseointegration have been decoupled via the analysis of *in vivo* performance for the placed Ti
17
18 implant with different surfaces. The developed Ti implant shows significantly improved
19
20 osseointegration with excellent bone-implant contact, improved mineralization of extracellular
21
22 matrix (ECM), and increased push-out force. These results suggest that the synergistic strategy of
23
24 combing electrical bioactivity with hierarchical surface structure provides a new platform for
25
26 developing advanced endosseous implants.
27
28
29
30
31
32
33
34
35
36
37

38 INTRODUCTION

39
40 Ti metal has gained worldwide recognition as one of the most acceptable candidates for
41
42 load-bearing bone repair materials.¹ However, the osseointegration of Ti implants is often
43
44 compromised due to the stress shielding effect and its bio-inertness.^{2,3} In particular, the lack of
45
46 mechanical stimulation to bone caused by the stress shielding effect and the poor bone-implant
47
48 bonding due to the generation of soft tissue on bio-inert pure Ti surface would directly lead to the
49
50 osteoporosis around the implantation site. Consequently, it eventually results in the failure of the
51
52 implant.⁴⁻⁶ As a living tissue, bone can remodel itself around the implantation site to adapt to the
53
54
55
56
57
58
59
60

1
2
3
4 new mechanical environment based on the structure of placed implant.⁷ This process is
5
6 accomplished by assembly of osteoblasts and osteoclasts into functional units, named as basic
7
8 multicellular units (BMUs).⁸ Because the implant surface directly touches with the surrounding
9
10 environment after surgery, the behavior of cells in the BMUs could be mediated by the surface of
11
12 implant. Thus, great efforts have been devoted to modifying the structure and surface of Ti
13
14 implant for improving osseointegration.⁹
15
16
17
18

19
20 Depending on the mechanical properties of composite material, the gradient stress
21
22 distribution corresponding to hierarchically porous surface of implant with bone tissue could
23
24 alleviate the stress shielding effect. To obtain the interlocking effect between the implant and
25
26 bone tissue, the size of gouges on the implant surface should be larger than 50 μm , which can
27
28 provide enough space for bone ingrowth based on the osseosynthesis.¹⁰ The fabrication of
29
30 hierarchically porous surface with excellent bonding to Ti implant is key to ensure the success of
31
32 the implant in load-bearing bone repair. Fortunately, the porous surface of TiO_2 coating formed
33
34 by microarc oxidation (MAO) can be regulated by controlling applied parameter, and the
35
36 as-formed coating exhibits excellent bonding with Ti substrate.¹¹⁻¹³ Therefore, a multi-scale
37
38 porous TiO_2 surface with micro gouges and sub-micro pores has been developed on Ti implant
39
40 via MAO, which enhances mechanical stimulation for improving osseointegration based on the
41
42 topographic cue from hierarchically structured surface to transmit load. Though the Ti implant
43
44 with certain hierarchical surface structure exhibits an enhancement in push-out force, soft tissue
45
46 is still partially covered the implant due to the poor bioactivity of the surface.¹⁴
47
48
49
50
51
52
53
54
55

56 In order to achieve a good osseointegration after implantation, numerous strategies have
57
58
59
60

1
2
3
4 been developed to facilitate Ti surface with good bioactivity.¹⁵⁻²⁰ Though chemical and
5
6 topographical-based coatings are the most promising approaches to render Ti surface with
7
8 excellent *in vivo* performance,¹⁷⁻¹⁹ their effects to bone tissue around the implantation site are
9
10 still limited if they have indirect contact with implant surface. Considering the stress shielding
11
12 effect, osteoporosis would easily occur in certain areas. It is known that bone is a piezoelectric
13
14 material, in which electric cue offered by externally applied electrical fields can modulate
15
16 osteoblastic cell behavior.^{21,22} Since the bone tissue can conduct electrical signal, the electric cue
17
18 could not only affect the contact interface but also influence the indirectly-contacted surrounding
19
20 area of the implant. However, electric cue provided by an external equipment is impractical for
21
22 orthopedic implant application.²³ To realize such a concept, developing Ti implant with an
23
24 internally built-in electrical field would be critical for the next-generation of implant.²³⁻²⁵
25
26
27
28
29
30
31

32 A promising strategy for the fabrication of such an internally built-in electrical field is based
33
34 on the concept of heterojunction, which promotes the separation of hole-electron pairs.²⁵⁻²⁷
35
36 Meanwhile, because of the electric coupling among different electrical fields,²⁸ the
37
38 heterojunction with the built-in electrical field can continuously provide electric cue to ensure a
39
40 long-term effect of the electrical bioactivity based on the response to varied electrical field from
41
42 piezoelectric bone during movement.²⁹ Interestingly, a built-in electrical field on smooth Ti plate
43
44 via the formation of bi-layered SnO₂-TiO₂ heterojunction with type II band alignment was
45
46 reported in our previous work, which exhibited superhydrophilicity and good apatite-forming
47
48 ability.³⁰ To render the hierarchically porous Ti implant with excellent bioactivity, in this work,
49
50 the bi-layered SnO₂-TiO₂ heterojunction was fabricated on the surface of hierarchically
51
52
53
54
55
56
57
58
59
60

structured Ti implant by MAO and subsequent hydrothermal treatment.

Because the individual TiO_2 or SnO_2 coating with an uniform surface does not exhibit bioactivity induced by electric cue, it provides a platform to decouple the effects of electric cue and topographic cue to osseointegration via the comparison of the bone remodeling, bone-implant interface, and biomechanical property for the prepared Ti implants with different surface structures.

RESULTS AND DISCUSSION

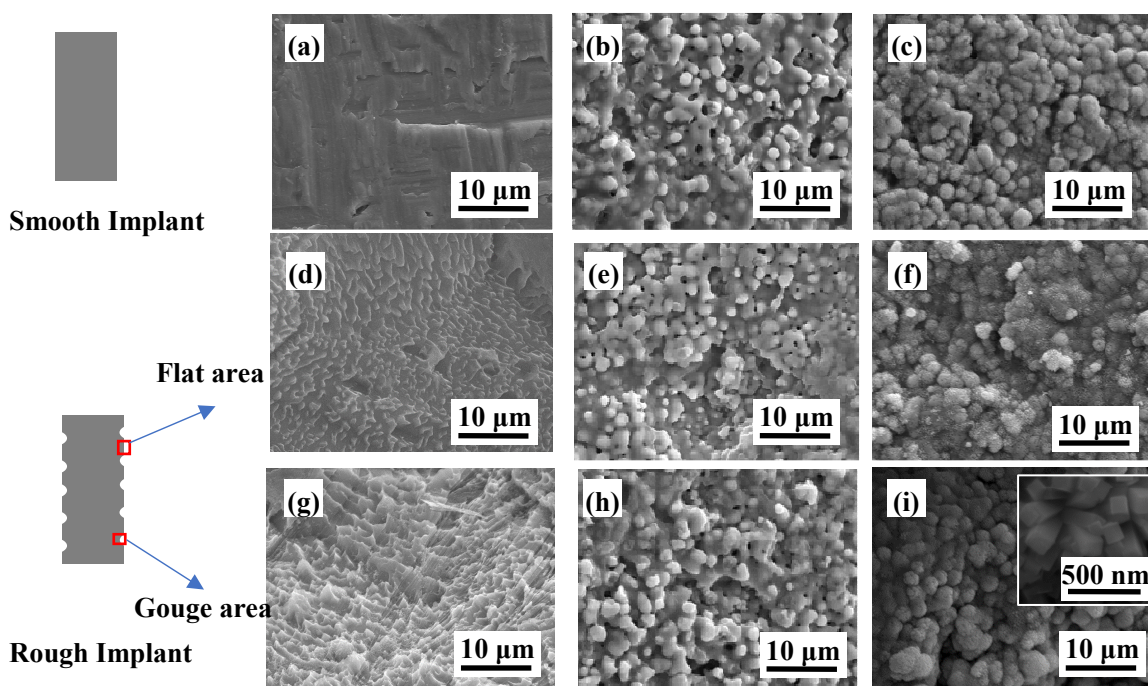


Figure 1 Surface morphologies of modified Ti implants with different structures: a) Ti, b) Ti-TiO₂, c) Ti-TiO₂-SnO₂; flat area of d) R-Ti, e) R-Ti-TiO₂, f) R-Ti-TiO₂-SnO₂; and gouge area of g) R-Ti, h) R-Ti-TiO₂, i) R-Ti-TiO₂-SnO₂.

To ensure a uniform structure of the developed coating at the different areas (flat area and

1
2
3
4 gouges area) of the implant, the Ti implant surface with micro gouges has been acidly etched to
5
6 remove the non-uniform oxide film before subsequent treatments. The reason for the acid etching
7
8 is that the non-uniform oxide film would lead to changes in morphology and phase composition
9
10 of the as-formed MAO coating in the different areas according to our previous investigation.³¹
11
12 As shown in Figure 1, the surface with a morphology of acidly etched pits has been formed on
13
14 the surface of rough Ti implant in both flat and gouge area. According to the EDS results, there is
15
16 no oxide film left on the implant surface (Figure S1). Therefore, the reaction during the
17
18 subsequent MAO treatment to the implant could occur homogeneously in both flat and gouge
19
20 areas, retaining to uniform surface morphology on the whole surface. A sub-micro porous layer
21
22 after MAO treatment (Figure 1(b,e,h)) and a layer of nanorod array after hydrothermal treatment
23
24 (Figure 1(i) and S2) are observed. In the following, the implants are labeled according to their
25
26 structure as shown in Table S1, which is divided into two groups, smooth group (Ti, Ti-TiO₂,
27
28 Ti-TiO₂-SnO₂) and rough group (R-Ti, R-Ti-TiO₂, R-Ti-TiO₂-SnO₂), based on the different
29
30 surface structures. Owing to the generation of gouges on the rough implant, a mass loss of the
31
32 implants has been measured, showing the porosity of the rough implants is $18.2 \pm 0.2\%$ (Figure
33
34 S3).
35
36
37
38
39
40
41
42
43
44
45
46
47
48
49
50
51
52
53
54
55
56
57
58
59
60

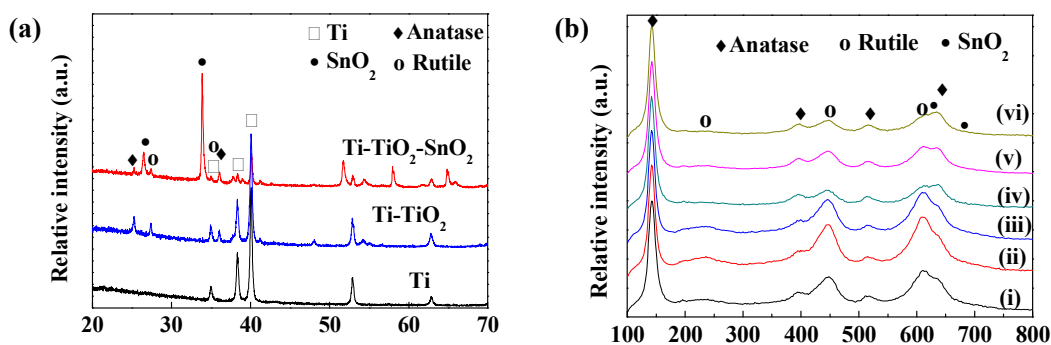
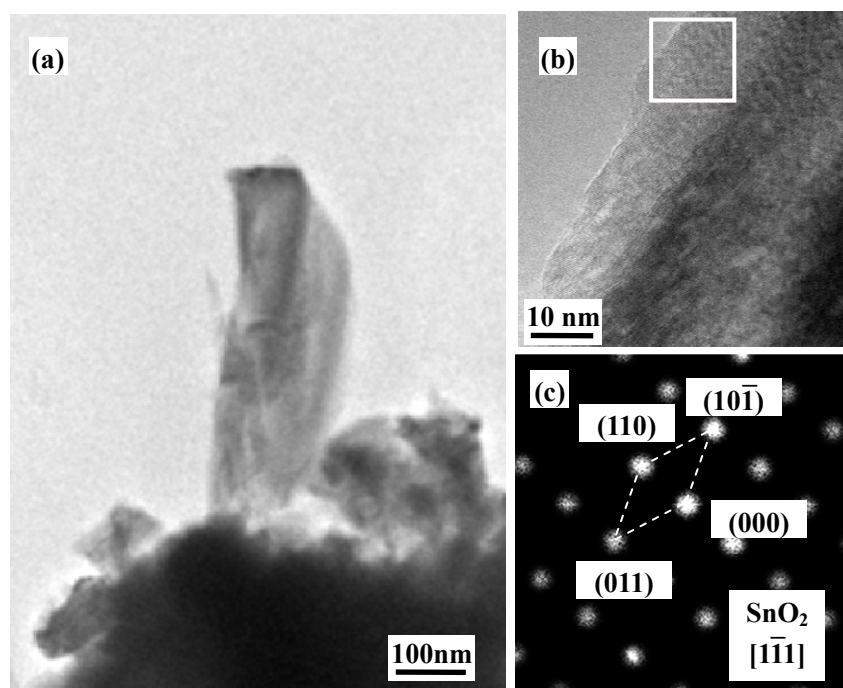


Figure 2 a) XRD patterns of Ti, Ti-TiO₂ and Ti-TiO₂-SnO₂; b) Raman spectra of coated implants detected from different area: i) Ti-TiO₂, ii) flat area of R-Ti-TiO₂, iii) gouge area of R-Ti-TiO₂, iv) Ti-TiO₂-SnO₂, v) flat area of R-Ti-TiO₂-SnO₂, and vi) gouge area of R-Ti-TiO₂-SnO₂.

Regarding the heterojunction, the crystallinity of designed phase is the key to its performance.³²⁻³⁴ The amorphous MAO coating with SnO₂ film cannot form a heterojunction with electrically stimulated bioactivity because it cannot obtain a stable Fermi energy of TiO₂ to promote the separation of hole-electron pairs.³⁰ To meet the formation requirement of heterojunction with type II aligned structure,^{35,36} a high voltage had to be applied to fabricate the MAO coating with good crystallinity. As expected, TiO₂ based MAO coating and the SnO₂ film were formed on Ti substrate after the subsequent treatments as indicated in the XRD patterns (Figure 2(a)).

To further confirm the phase composition of the coating generated on the implant with micro gouges, Raman spectroscopy has been employed to characterize the coating in both gouges area and flat area. Consistent with the XRD results, similar Raman spectra of the MAO coating with two different phases of TiO₂ have been detected from different areas of Ti-TiO₂ and R-Ti-TiO₂,

1
2
3
4 revealing that the gouge does not affect the phase composition of MAO coating (Figure 2(b)).
5
6 The Raman modes centered at 144, 399, 519 and 639 cm^{-1} are pointed to the anatase phase TiO_2 ,
7
8
9 ³⁷ while the Raman modes centered at 240, 446 and 609 cm^{-1} are assigned to the rutile phase
10
11 TiO_2 . ³⁸ As for the nanorods film, Raman spectra detected from both the gouge and flat areas
12
13 show similar characteristic vibration modes of SnO_2 , which are centered at 629 and 689 cm^{-1} , ³⁹
14
15 respectively (see in Figure S4). Both the XRD and Raman results indicate a uniform $\text{SnO}_2\text{-TiO}_2$
16
17 bi-layer was fabricated on the surface of $\text{Ti-TiO}_2\text{-SnO}_2$ and $\text{R-Ti-TiO}_2\text{-SnO}_2$, which is in good
18
19 bi-layer was fabricated on the surface of $\text{Ti-TiO}_2\text{-SnO}_2$ and $\text{R-Ti-TiO}_2\text{-SnO}_2$, which is in good
20
21 agreement with the bi-layered $\text{SnO}_2\text{-TiO}_2$ coating on Ti plate reported in our previous work. ³⁰
22
23



24
25
26
27
28
29
30
31
32
33
34
35
36
37
38
39
40
41
42
43
44
45
46
47 **Figure 3** a) the TEM morphology of the powder collected from $\text{R-Ti-TiO}_2\text{-SnO}_2$, b) high resolution TEM
48 morphology of nanorod and c) selected area electron diffraction pattern obtained by Fast Fourier Transform
49 morphology of nanorod and c) selected area electron diffraction pattern obtained by Fast Fourier Transform
50 morphology of nanorod and c) selected area electron diffraction pattern obtained by Fast Fourier Transform
51 morphology of nanorod and c) selected area electron diffraction pattern obtained by Fast Fourier Transform
52 morphology of nanorod and c) selected area electron diffraction pattern obtained by Fast Fourier Transform
53 morphology of nanorod and c) selected area electron diffraction pattern obtained by Fast Fourier Transform

54 To further confirm the structure of $\text{SnO}_2\text{-TiO}_2$ coating formed on the $\text{R-Ti-TiO}_2\text{-SnO}_2$, TEM
55
56
57
58
59
60

has been used to analyze the powder collected from its surface (Figure 3). Clearly, the nanorod is mainly composed of Sn and O as confirmed by the EDS results. The selected area electron diffraction (SAED) pattern of the nanorod obtained by the Fast Fourier Transform (FFT) technique further confirms its phase of SnO₂ (Figure 3 (c)). Thus, we can confirm that SnO₂ nanorods film was generated on the R-Ti-TiO₂-SnO₂ surface.

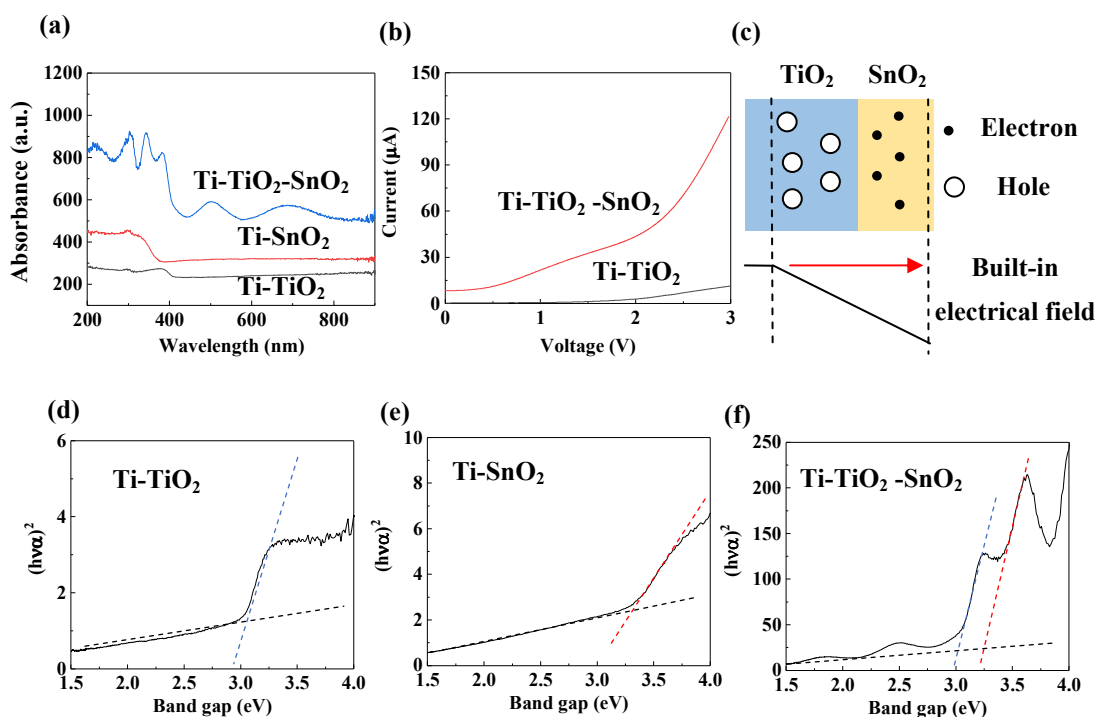


Figure 4 a) UV-vis absorption spectra of Ti-TiO₂, Ti-SnO₂, and Ti-TiO₂-SnO₂, b) LSV curves of Ti-TiO₂, and Ti-TiO₂-SnO₂, c) schematic diagram for the built-in electrical field of SnO₂-TiO₂ heterojunction, and the plots of $(ahv)^2$ versus hv of d) Ti-TiO₂, e) Ti-SnO₂, f) Ti-TiO₂-SnO₂.

Due to the similar phase composition and structure of the bi-layered SnO₂-TiO₂ coating with our previous work on Ti plate,³⁰ an n-n heterojunction could be formed on the R-Ti-TiO₂-SnO₂ surface. To confirm the formation of the SnO₂-TiO₂ heterojunction, the band gap of the

1
2
3
4 bi-layered SnO₂-TiO₂ coating has been determined by UV-vis spectrophotometer using Ultra
5
6 Violet Diffuse Reflectance Spectroscopy technique (Figure 4). Based on the UV absorption
7
8 spectral data, the direct band gaps can be obtained by Tauc relation with a linear fit via the
9
10 equation: ⁴⁰ $(\alpha hv)^2 = A \cdot (hv - E_g)$, where α is absorption coefficient, A is the proportionality
11
12 constant, hv is the photon energy, and E_g is the energy band gap. Clearly, individual TiO₂ or
13
14 SnO₂ film shows typical semi-conductor feature, with the calculated band gap of 3.01 and 3.38
15
16 eV, respectively. As for the Ti-TiO₂-SnO₂, the band gaps of both TiO₂ layer and SnO₂ layer are
17
18 observed, indicating the formation of SnO₂-TiO₂ heterojunction. Interestingly, two peaks around
19
20 700 and 510 nm are also observed in the UV-vis absorption spectrum of Ti-TiO₂-SnO₂ (Figure
21
22 4(a)), indicating that electrons on Ti-TiO₂-SnO₂ surface can transfer to conduction band (CB)
23
24 with lower excited energy than that of individual TiO₂ or SnO₂. This result further confirms the
25
26 formation of SnO₂-TiO₂ heterojunction, because the separated electrons and holes with the
27
28 metastable status have already been stimulated by the built-in electrical field of heterojunction,
29
30 resulting in the reduced energy for photoelectronic excitation to overcome the energy barrier. In
31
32 addition, according to Figure 4(b), the Linear sweep voltammetry (LSV) curve of the
33
34 Ti-TiO₂-SnO₂ coating shows significantly larger response current than that of the Ti-TiO₂,
35
36 suggesting better electrical conductivity of the coating due to the formation of heterojunction
37
38 thus higher charge carrier density. Such SnO₂-TiO₂ coating exhibits superhydrophilicity, good
39
40 apatite-forming ability, and negative surface potential, leading to good electrical bioactivity.³⁰
41
42
43
44
45
46
47
48
49
50
51
52
53 Combined with the hierarchical structure of Ti implant, the synergistic effect of hierarchical
54
55 surface structure and electrical bioactivity for the developed Ti implants on osseointegration has
56
57
58
59
60

1
2
3
4 been investigated.
5

6 Normally, bone is considered as a dynamic living tissue which is constantly being remodeled
7 throughout its lifetime, it can adapt its mass and architecture to mechanical demands according
8 to the Wolff's law.⁴¹ To evaluate the status of bone remodeling around the placed Ti implants
9 with different surface structure, the biological tissue around the implants in the region of interest
10 (ROI) ($\Phi 3 \times L6 \text{ mm}^3$) have been analyzed by micro-CT after healing for 12 weeks.
11
12
13
14
15
16
17
18
19
20
21
22
23
24
25
26
27
28
29
30
31
32
33
34
35
36
37
38
39
40
41
42
43
44
45
46
47
48
49
50
51
52
53
54
55
56
57
58
59
60

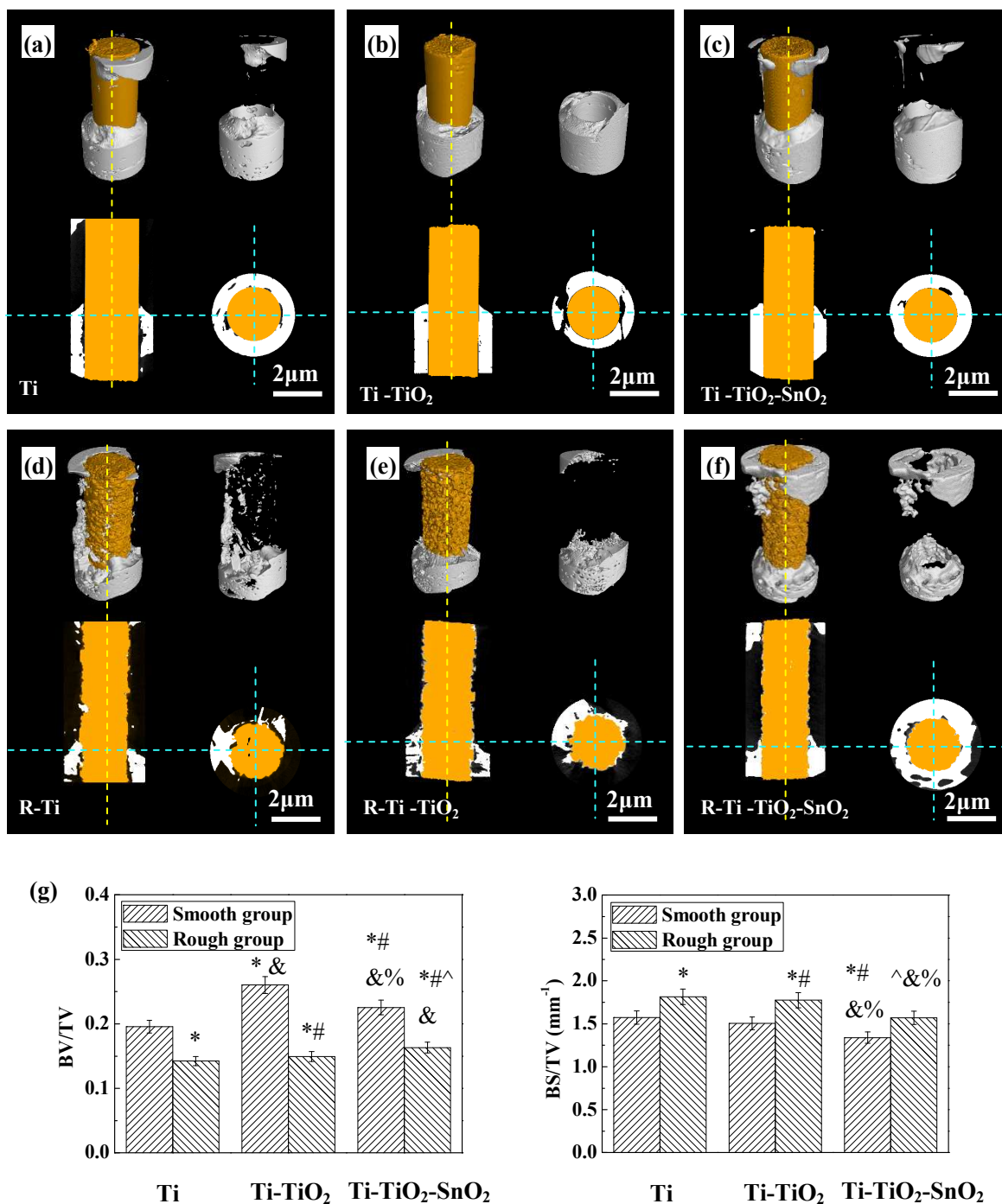


Figure 5 Micro-CT analysis of the biological tissue around implants after surgery for 12 weeks: micro-CT images of a) Ti, b) Ti-TiO₂, c) Ti-TiO₂-SnO₂, d) R-Ti, e) R-Ti-TiO₂, f) R-Ti-TiO₂-SnO₂, and g) the morphometric results in the ROI. *p < 0.05 compared to the Ti implant, #p < 0.05 compared to the Ti-TiO₂, ^p

1
2
3
4 < 0.05 compared to the Ti-TiO₂-SnO₂, &p < 0.05 compared to the R-Ti, %p < 0.05 compared to the R-Ti-TiO₂.
5

6
7 According to the cross-sectional morphology of the reconstructed micro-CT images, the
8
9 biological tissue exhibits a trend to grow along the implant surface towards the marrow cavity
10
11 (Figure 5). Meanwhile, the biological tissue-implant interface of both the smooth and rough
12
13 groups shows a similar status with the varied surface structures (the indirect contact for Ti and
14
15 R-Ti, the partial direct contact for Ti-TiO₂ and R-Ti-TiO₂, and the almost perfect direct contact
16
17 for Ti-TiO₂-SnO₂ and R-Ti-TiO₂-SnO₂). As for the Ti and R-Ti implants, they are separated from
18
19 the biologic tissue by gaps due to the bio-inert nature of pure Ti, leading to the indirect contact
20
21 with bone. Therefore, they both show the least amount of remodeling biological tissue around the
22
23 implant (Figure 5(a,d)). With regard to the Ti-TiO₂ and R-Ti-TiO₂, the biological tissue partially
24
25 contacts with the implant surface, while cavities also appear in the bone near certain area (Figure
26
27 5(b,e)). The formation of the cavities could be attributed to the stress shielding effect between the
28
29 implant and bone, which stimulates osteoclasts to resorb more bone in the decreased levels of
30
31 stress direction.⁷ However, owing to the relatively better bioactivity of TiO₂ coating than that of
32
33 pure Ti, new biological tissue has been generated toward the direction of marrow cavity around
34
35 the implant to ensure load bearing capability during the bone healing process. Nevertheless, it
36
37 still shows a relatively loose structure around R-Ti-TiO₂ (Figure 5e). This is strongly supported
38
39 by the additional statistical analysis for the ROI (Figure 5(g)), where biological tissue with large
40
41 surface area is obtained, indicating more cavities are detected from the biological tissue around
42
43 the implant when compared with the R-Ti-TiO₂-SnO₂. In the case of the implants with
44
45 SnO₂-TiO₂ bi-layered coating, they exhibit the densest structure with excellent biological
46
47
48
49
50
51
52
53
54
55
56
57
58
59
60

tissue-implant contact. The reason for this is attributed to the electrical bioactivity of the coating, which benefits not only the directly contacted tissue, but also the surrounding tissues due to the effect of electrical field.

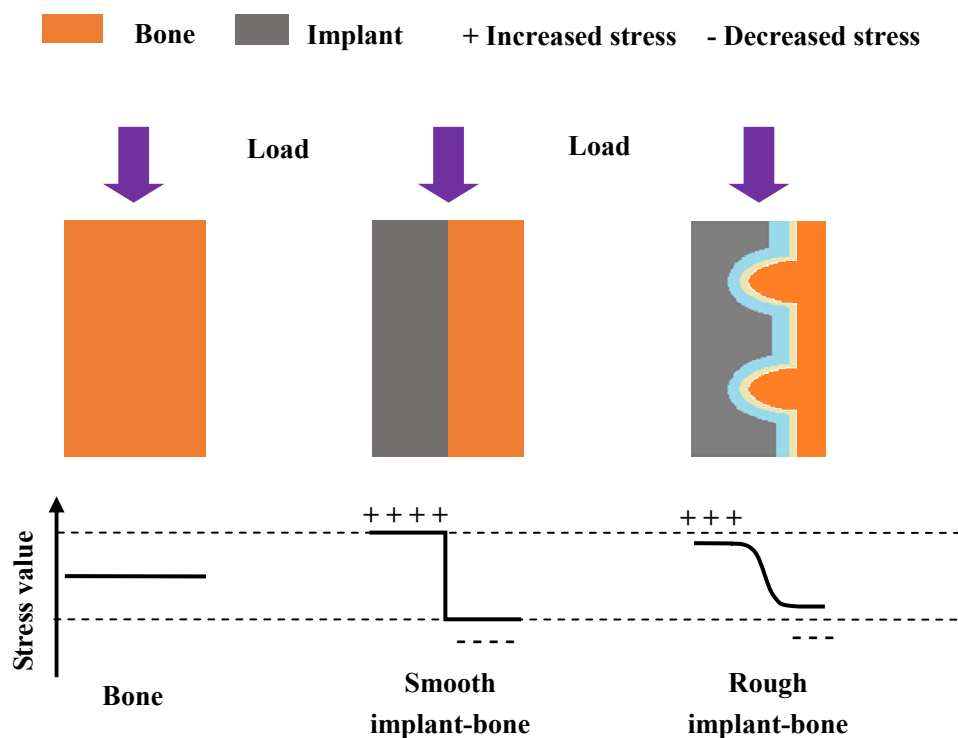


Figure 6 Schematic diagram for the stress distribution at the interface between bone and implants along the radial direction.

Apparently, the structure of biological tissue around the placed implant after healing of 12 weeks depends on the hierarchical structure of the implant surface (Figure 5). This is in agreement with the result that the stress distribution within the bone tissue is related to the recruitment and activity of BMU.^{7,42} After the ingrowth of new bone into the micro scale gouges, the placed implant with surrounding bone tissue can be considered as a composite material, which significantly changes the stress distribution in the bonding area (Figure 6). During the

1
2
3
4 remodeling process in cortical bone, osteoclasts could be observed on the surface of an area with
5
6 reduced stress, and osteoblasts could be found on the surface of an area with increased stress.^{7,42}
7
8

9 If a material is with hierarchical bonding interface, the stress on the bone tissue side is decreased
10
11 but with an increasing trend toward the interface to implant. The decreased stress could promote
12
13 osteoclast to resorb bone along certain direction, while the increase of stress could stimulate
14
15 osteoblast to aid remodeling at the interface.⁴³ Thus, more cavities but better bone-biological
16
17 contact were observed around the R-Ti and R-Ti-TiO₂ when compared with the smooth group.
18
19
20
21

22 Because of the existence of artifacts, soft tissue and mineral bone are hard to be
23
24 distinguished by the Micro-CT analysis. To further support our point about the BMU coupling,
25
26 histological morphometry of the Van Gieson (VG) stained bone tissue within 500 μm to the
27
28 surface of implant has been investigated (Figure 7). Apparently, the cavities containing
29
30 osteoclast and osteoblast can be clearly observed in the magnified histological morphology
31
32 around implants. As the functional unit for bone remodeling, BMUs is considered as the most
33
34 obvious agent to adjust and reveal the bone healing situation around the implant surface in micro
35
36 scale.⁴⁴⁻⁴⁸ Disturbances of any stimulation that shift the equilibrium of BMUs would lead to the
37
38 change in bone remodeling around implants.⁴⁹ Herein, the change in size of cavity containing
39
40
41
42
43
44
45
46
47
48
49
50
51
52
53
54
55
56
57
58
59
60
BMU is mainly attributed to two factors of the as-formed implants, the bioactivity of coating and
the micro gouge structure.

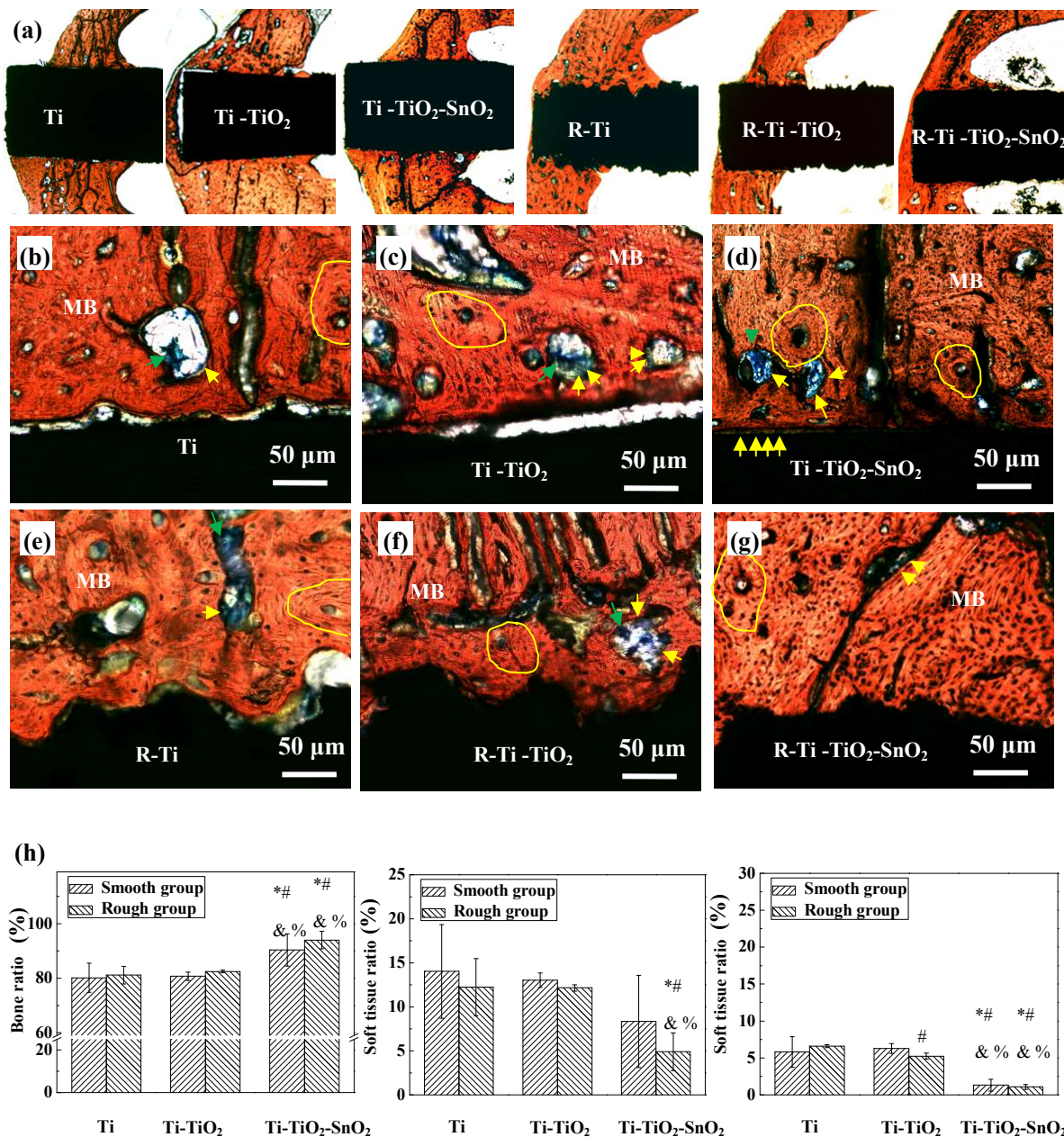


Figure 7 Histological analysis of the bone around the implants after surgery for 12 weeks: a) gross morphologies of the VG stained bone tissue around implants, the representative histological morphology of b) Ti, c) Ti-TiO₂, d) Ti-TiO₂-SnO₂, e) R-Ti, f) R-Ti-TiO₂, g) R-Ti-TiO₂-SnO₂, and h) the histomorphometric results of mineralized bone, soft tissue and gap in the interested zoon. (yellow arrow) osteoblasts; (green arrow) osteoclasts; (yellow ring) osteon; (MB) mineralized bone. **p* < 0.05 compared to the Ti implant, #*p* < 0.05

1
2
3
4 compared to the Ti-TiO₂, [^]p < 0.05 compared to the Ti-TiO₂-SnO₂, &p < 0.05 compared to the R-Ti, %p < 0.05
5
6 compared to the R-Ti-TiO₂.
7

8
9 As for the smooth surface group, the behavior of BMUs is dominated by the bioactivity of
10 the implant surface. Generally, the equilibrium of BMUs around implants shifts towards bone
11 resorption after implantation, due to the decrease of stress stimulation to bone tissue caused by
12 the stress shielding effect. Regarding the Ti implant, the surrounding tissue normally shows
13 osteoporosis due to the bio-inertness of pure Ti (Figure 7(b)), which is unable to promote
14 osteoblastic functions (such as proliferation, migration, differentiation, secretion of matrix
15 proteins, and its mineralization) to rebalance the equilibrium of BMUs.⁵⁰
16
17
18
19
20
21
22
23
24
25

26
27 In terms of Ti-TiO₂, the MAO coating with porous surface structure in sub-micro scale can
28 enhance the proliferation and differentiation of osteoblasts.⁵¹ Meanwhile, the TiO₂ coating with
29 negative surface charges can attract Ca²⁺ and proteins absorption.⁵² They all shift the
30 equilibrium of BMUs around the implant surface towards the bone generation, playing a positive
31 role in osseointegration. Thus, a direct bone-implant contact has been observed around the
32 implant surface near the marrow cavity (Figure 7(c)). However, because of the relatively weak
33 Ca²⁺ attraction for TiO₂ surface and the indirect contact of the surface with both the cell and
34 proteins from medullary cavity fluid, some surface of the Ti-TiO₂ is still partially separated by
35 gaps or soft tissue near the implantation site. It should be noticed that cavities with osteoclast cell
36 have also been observed in the indirectly contacted bone tissue around Ti-TiO₂ (Figure 7(c)),
37 indicating that the positive effect of the MAO coating on BMUs for bone generation is only
38 limited in the directly contacted area.
39
40
41
42
43
44
45
46
47
48
49
50
51
52
53
54
55
56
57
58
59
60

1
2
3
4 Though the Ti-TiO₂-SnO₂ shows similar surface roughness with Ti-TiO₂, the equilibrium of
5
6 BMUs around it shifts significantly towards the generation of new bone. This phenomenon is
7
8 obviously dominated by the electrical bioactivity of the bi-layered coating rather than the
9
10 nano-topography of the SnO₂ surface, as the densely packed SnO₂ nanorods would not benefit
11
12 focal adhesion assembly of cells.^{30,53,54} Specifically, transient receptor potential melastatin 7
13
14 (TRPM7) protein is one of the signaling pathways on plasma membranes, exhibiting
15
16 spontaneously activated divalent cation (Ca²⁺, Mg²⁺) entry, which is important for osteoblast
17
18 differentiation.^{55,56} Because the surface of SnO₂-TiO₂ heterojunction with negative zeta potential
19
20 can attract Ca²⁺ and Mg²⁺ absorption,³⁰ the functional activity of TRPM7 would be ensured
21
22 under the culture conditions with high intracellular Ca²⁺ or Mg²⁺ concentrations, benefiting the
23
24 osteoblast differentiation of mesenchymal stem cells around implant.^{57,58} Therefore, a cement
25
26 line interface has been observed on the surface Ti-TiO₂-SnO₂ (Figure 7(d)). Meanwhile, larger
27
28 amount of osteoblast cells has been proliferated in the cavities around Ti-TiO₂-SnO₂ when
29
30 compared with the others.
31
32
33
34
35
36
37
38

39
40 Regarding to the rough implants with micro gouge structure, it is obvious that the
41
42 osseointegration has improved when compared with the smooth surface with the same modified
43
44 coating (Figure 7). This is attributed to the changes in the absorption of cells and proteins and the
45
46 topographic cue for the surrounding tissue based on the implant structure. Firstly, the migration
47
48 and proliferation of osteoblast or stem cell and absorption of matrix proteins has been accelerated
49
50 by the gouges surface structure because of its storage ability for the medullar cavity liquid.
51
52
53
54
55
56 Secondly, the space provided by surface gouges changes the topographic cue to the surrounding
57
58
59
60

bone tissue. The micro gouges are very similar to the structure of proceed osteonal tunneling with BMUs, which would be quickly refilled by osteoblast.⁷ Thus, the equilibrium of BMUs around the rough implants with micro gouges shifts towards the bone formation.

Associated with the electrical bioactivity of SnO₂-TiO₂ coating and the surface gouge structure, the attraction of Mg²⁺ and Ca²⁺ by the built-in electrical field would be significantly enhanced by the superposition of the electrical field based on the micro gouges structure. Thus, more Mg²⁺ and Ca²⁺ would enrich around the Ti-TiO₂-SnO₂ surface. It could ensure the functional activity of TRPM7,^{57,58} showing excellent osseointegration around the implant (Figure 7(g)).

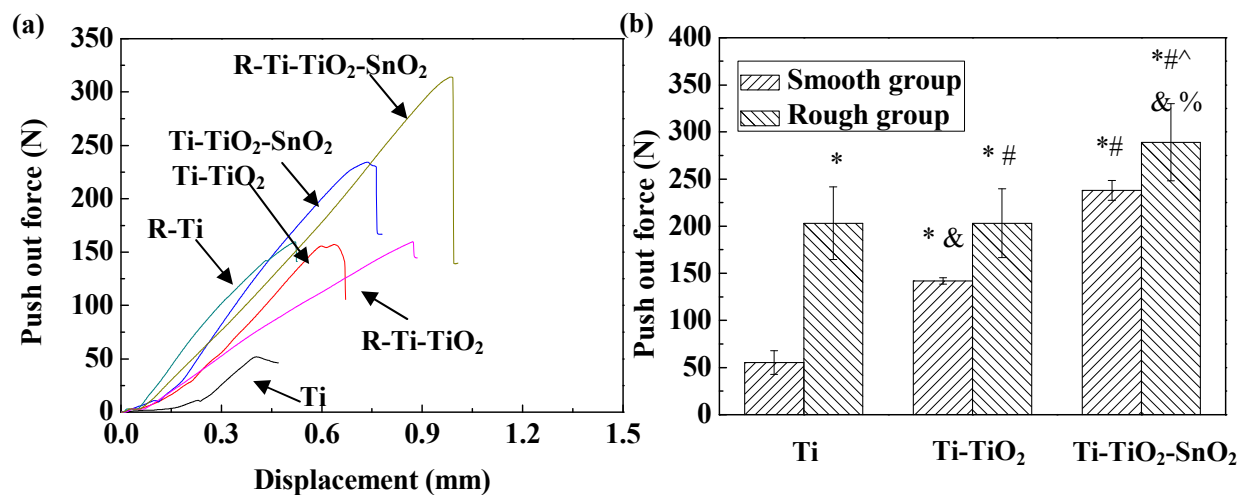


Figure 8 Biomechanical results of the implants after surgery for 12 weeks: a) the typical displacement curves of the implants during the push-out process, b) the push-out force of the implants with different surface structures. * $p < 0.05$ compared to the Ti implant, # $p < 0.05$ compared to the Ti-TiO₂, ^ $p < 0.05$ compared to the Ti-TiO₂-SnO₂, & $p < 0.05$ compared to the R-Ti, % $p < 0.05$ compared to the R-Ti-TiO₂.

To evaluate the long-term bonding between the developed implant and bone tissue, the

1
2
3
4 push-out forces for the implants after healing of 12 weeks have been studied (Figure 8). As
5
6 expected, both the electrically bioactive coating and the gouges structure surface exhibit an
7
8 increase in the push-out force. In the case of the smooth implant group, the enhancement in the
9
10 push-out force is dominated by the bioactivity of the implant surface. Obviously, the push-out
11
12 force of the implant with SnO₂-TiO₂ is significantly improved to 239 N, which is over 5 times
13
14 that of the pure Ti (50 N) (p<0.05). As for the rough implants with micro gouges, though it has
15
16 less amount of remodeled bone around the implants, they exhibit much higher push-out force
17
18 than the smooth ones (Figure 8). In consistent with our previous work,¹⁴ no matter how the
19
20 bone-implant contact is, the push-out force for R-Ti and R-Ti-TiO₂ is similar. The reason for this
21
22 could be attributed to the meshed bone-implant interface, which changed the failure mode of the
23
24 implant when compared with the smooth ones. Interestingly, the push-out force of
25
26 R-Ti-TiO₂-SnO₂ is further increased to 289 N, which is much stronger than that of R-Ti-TiO₂ and
27
28 R-Ti. This supports our analysis that the electrical bioactivity benefits the osteoblastic function,
29
30 leading to increased mineralization of extra-cellular matrix (ECM) around the developed implant
31
32 to transmit load efficiently.
33
34
35
36
37
38
39
40
41
42
43
44
45
46
47
48
49
50
51
52
53
54
55
56
57
58
59
60

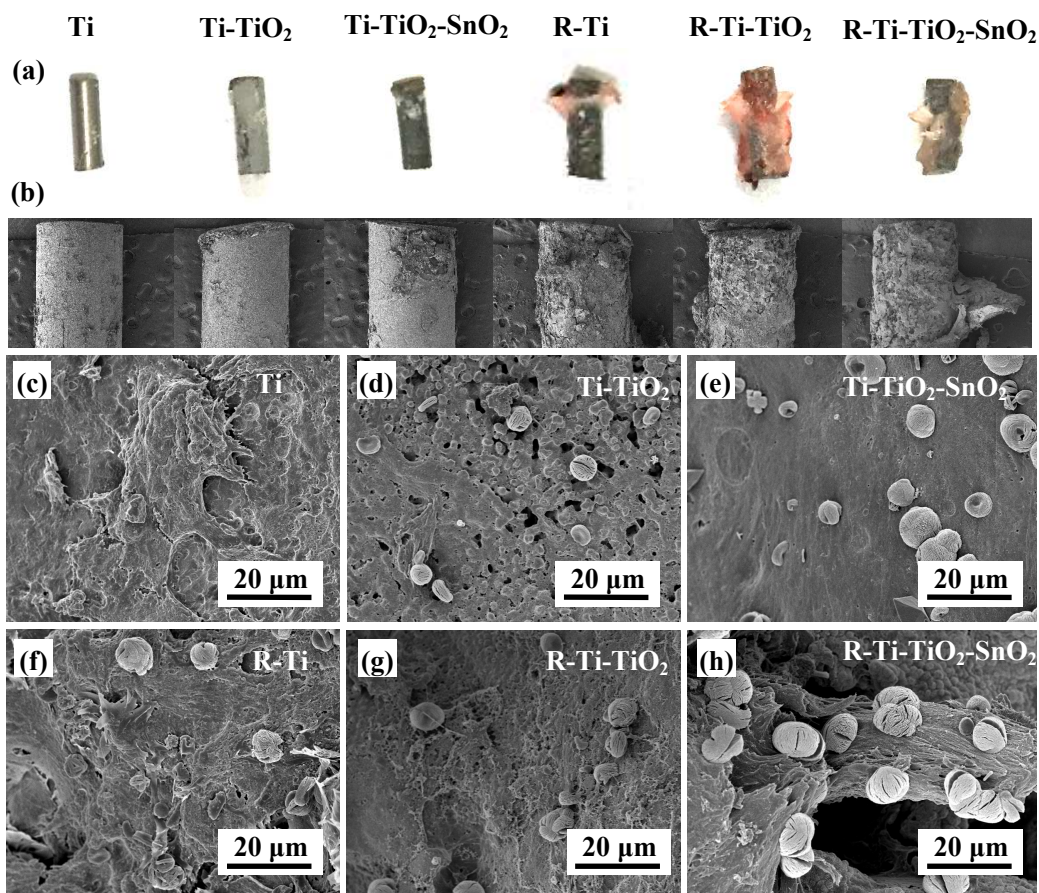


Figure 9 Surface morphologies of the pushed-out implants after healing of 12 weeks: a) gross images of the pushed-out implants, b) SEM images of the pushed-out implant surfaces with biological tissue at the cortical bone area, magnified SEM morphologies of the implant surface c) Ti, d) Ti-TiO₂, e) Ti-TiO₂-SnO₂, f) R-Ti, g) R-Ti-TiO₂, h) R-Ti-TiO₂-SnO₂.

To confirm the failure mode of the implants, representative SEM images of the pushed-out implant in the cortical regions are investigated together with EDS. Clearly, larger amount of biological tissue with meshed structure is observed on the rough implant surfaces compared to the smooth ones (Figure 9). As for the smooth group, pure Ti implant is partially covered by soft tissue, leading to poor contact with surrounding bone tissue, while some deposition with the

1
2
3
4 shape of distorted sphere in multi-flakes (Ca 14.1 wt. % and P 1.4 wt. %) have been observed on
5
6 the Ti-TiO₂ surface because of its bioactivity. As expected, a large amount of remnants bone (Ca
7
8 78.5 wt. % and P 12.2 wt. %) and sphere-like deposition (Ca 27.2 wt. % and P 6.1 wt. %) have
9
10 been observed on the surface of Ti-TiO₂-SnO₂. The above evidence directly supports our analysis
11
12 that the electrically bioactive coating can significantly improve the mineralization of the
13
14 remodeled bone tissue through the attraction of Mg²⁺ and Ca²⁺, providing ions signal via the path
15
16 way of TRM7 on the plasma membrane to accelerate the osteoblastic functions. Further analysis
17
18 on the fracture morphology in the cortical bone area of the implant shows that some part of the
19
20 coating on the Ti-TiO₂-SnO₂ has been pulled out with the bone tissue (Ti 78.8 wt. % and C 8.8
21
22 wt. %) (Figure S5), indicating the synostosis in the cortical region. As for the rough group, the
23
24 micro gouges on the R-Ti-TiO₂-SnO₂ surface around the cortical bone side are almost fully filled
25
26 by dense mineral bone, and fracture mainly occurs at the bone side with large amount of Ca, P
27
28 and Mg enriched sphere-like depositions (Figure 9). On the contrary, smaller amount of Ca, P
29
30 and Mg enriched sphere-like depositions has been observed on R-Ti-TiO₂. This result is in
31
32 agreement with Couchourel's suggestion that the culture conditions with low extracellular Mg²⁺
33
34 and Ca²⁺ concentrations promotes gene expression of collagen type I alpha 1, resulting in
35
36 reduced mineralization of ECM because of the abnormal ratio of matrix protein.⁵⁹ This further
37
38 supports our analysis that the electrical bioactivity provided by SnO₂-TiO₂ hetero-junction would
39
40 benefit the mineralization of the indirect contact bone tissue around the implant, resulting in a
41
42 significant improvement in osseointegration of the developed implant.
43
44
45
46
47
48
49
50
51
52
53
54

55
56 Recently many strategies have been developed to improve the osseointegration of Ti implant.
57
58
59
60

1
2
3
4 Compared with dense Ti implant, the scaffold Ti implant shows obviously enhanced push-out
5
6 force thanks to the three-dimensional inter-locking effect for the new bone which grows into the
7
8 holes after healing.^{10,60-63} Similar to the scaffold Ti implant, in this work, regenerated bone tissue
9
10 also meshed with the rough implant in the gouge areas. While, since the fixed porosity of the
11
12 rough implants limits the ingrowth of bone tissue, the further enhancement in push-out force of
13
14 R-Ti-TiO₂-SnO₂ is attributed to the increased mineralization of ECM around the implant with
15
16 synostosis. Comparing the push-out stress with the literature values (seeing in supporting
17
18 information Table S2), it suggests that the R-Ti-TiO₂-SnO₂ shows the most improved
19
20 performance, even better than that of surface chemically modified Ti scaffold. Taking the results
21
22 together, the R-Ti-TiO₂-SnO₂ with the synergistic effects of both electrical bioactivity and
23
24 hierarchical surface structure has been demonstrated as an efficient approach to enhance
25
26 osseointegration.
27
28
29
30
31
32
33
34
35
36
37

38 CONCLUSION

39
40 Hierarchically porous surface with SnO₂-TiO₂ heterojunction has been fabricated on Ti
41
42 implant. The significantly improved osseointegration is attributed to electrical bioactivity and
43
44 hierarchical surface structure of the developed implant. The electrical bioactivity rendered by the
45
46 bi-layered SnO₂-TiO₂ coating on the implant benefits not only the contacted biological tissue but
47
48 also the indirectly contacted one thanks to the generation of electrical signal. It improves the
49
50 osteoblastic function of BMUs, leading to increased mineralization of ECM around the implant
51
52 with synostosis. Thanks to the topographic cue from the hierarchically porous surface, the newly
53
54
55
56
57
58
59
60

1
2
3
4 formed bone tissue grows into the micro gouges of rough implant, exhibiting meshed
5
6 bone-implant interface. Meanwhile, the osteoblastic function of BMUs is improved compared to
7
8 the smooth ones, because the space provided by gouges can act as a storage of medullar cavity
9
10 liquid, promoting the absorption of matrix proteins and attachment of cells. Benefiting from the
11
12 superposition of the built-in electrical field provided by heterojunction on the hierarchically
13
14 porous surface, the mineralization of the remodeled bone around the developed Ti implant is
15
16 further enhanced, exhibiting excellent *in vivo* performance. Therefore, the concept of
17
18 hierarchically structured Ti implant with electrically bioactive surface could be a promising
19
20 approach for developing the next-generation of load-bearing Ti implants, since it benefits from
21
22 both electric and topographic cues to the living bone.
23
24
25
26
27
28
29
30
31

32 **EXPERIMENTAL SECTION**

33
34
35 **Surface modification.** The medical Ti rods with the size of $\Phi 2 \times L 6 \text{ mm}^3$ (Grade II, Baoji
36
37 Haibao special metal materials Co., China) were used as Ti implants for the surface modification
38
39 and animal surgery. Firstly, the rods were ground with 1000# abrasive paper, ultrasonically
40
41 washed with acetone, ethanol and distilled water. The micro scale gouges were prepared on Ti
42
43 implant surface via microarc oxidation (MAO) in an electrolyte containing NaNO_3 ($0.1 \text{ M}\cdot\text{L}^{-1}$)
44
45 and NaOH ($0.25 \text{ M}\cdot\text{L}^{-1}$) at 280 V for 2 min, then acidly washed in 48 wt.% H_2SO_4 at 80 °C for 2
46
47
48
49
50
51 h. To fabricate sub-micro scale porous coating on Ti, the implants were microarc oxidized in an
52
53 electrolyte containing EDTA-2Na ($0.04 \text{ M}\cdot\text{L}^{-1}$) and NaOH ($0.175 \text{ M}\cdot\text{L}^{-1}$) at 450 V for 5 min.
54
55
56 Next, the microarc oxidized implants were hung in a PTFE cup but soaked with 40 mL bulk
57
58
59
60

1
2
3
4 solution (distilled water 30 mL and ethanol 10 mL) containing 0.7 g of NaOH and 0.5 g of
5
6 $\text{SnCl}_4 \cdot 5\text{H}_2\text{O}$. Then, the steel vessel containing the PTFE cup were treated at 200 °C for 24 h. The
7
8 surface modified implants were labelled according to the surface structure (Table S1).
9

10
11 **Surface characterization.** Surface morphology of the implants was observed by scanning
12
13 electron microscopy (SEM, Helios Nanolab 600i, FEI Co., USA). The elemental composition of
14
15 the surface with different features was investigated by an energy dispersive X-ray spectrometer
16
17 (EDAX, USA) equipped with the SEM system. X-ray diffraction (XRD, D/max-gB, Japan) and
18
19 Raman spectroscopy (Raman, Jobin Yvon, France) were used to analyze the phase composition
20
21 of the smooth and rough implants, respectively. The phase and elemental composition of the
22
23 nanorod formed on R-Ti-TiO₂-SnO₂ surface was further analyzed by transmission electron
24
25 microscopy (TEM, Tecnai G2F30, FEI Co., USA) instrument via high resolution TEM and EDS.
26
27 Reflectance spectra from 900-200 nm were recorded via UV-vis spectrophotometer (UV-2600,
28
29 Shimadzu, Japan) to calculate the band gap for the semi-conductor layer on Ti-TiO₂, Ti-SnO₂ and
30
31 Ti-TiO₂-SnO₂. The LSV curves of the samples were scanned from 0 V to 3 V versus SCE
32
33 (saturated calomel reference electrode) by electrochemical workstation (CHI760E,
34
35 Shanghai Chenhua Instrument, China), and 0.5 M Na₂SO₄ was used as the electrolyte.
36
37

38
39 ***In vivo* Experiments.** All the animal experiments were approved by the animal care and
40
41 experiment committee of Xi'an Jiaotong University College of Medicine complied with the
42
43 approved guidelines. The detailed animal experimental methods have been reported in our
44
45 previous works.^{14,30,50} Twelve New Zealand rabbits (2.5–3 kg for each) were used in this work.
46
47
48 During the surgery, three holes ($\Phi 2 \times L6 \text{ mm}^3$) were drilled on each tibia of rabbit. And the Ti,
49
50
51
52
53
54
55
56
57
58
59
60

1
2
3
4 Ti-TiO₂ and Ti-TiO₂-SnO₂ implants were placed on the left leg, while the R-Ti, R-Ti-TiO₂ and
5
6
7 R-Ti-TiO₂-SnO₂ were placed on the right leg (Figure S6).

8
9 After healing of 12 weeks, the rabbits were sacrificed to investigate the osseointegration of
10
11 implants with different surface structures. X-ray 3D imaging system (Y. Cheetah, YXLON
12
13 International GmbH, Germany) was used to rebuild the biological tissue around the implants in
14
15 the region of interest (ROI) ($\Phi 3 \times L6 \text{ mm}^3$) with an isotropic resolution of 8 μm . For
16
17 morphometric measurement in ROI, the biological tissue volume (BV), total volume without the
18
19 implant (TV) and biological tissue surface area (BS) were analyzed by VG Studio 2.1V. The Van
20
21 Gieson (VG) stained transverse histological sections were observed by OLYMPUS microscope
22
23 (CXX41, OLYMPUS, Japan) with a normal light source. The histomorphometrical measurement
24
25 of the bone tissue with a distance of 500 μm to the cylindrical surface of implant was analyzed
26
27 by ImageJ (Figure S7). The push-out force of the placed implants was measured by a universal
28
29 testing machine (Instron-1186, Instron Co., USA).

30
31
32
33
34
35
36
37
38 **Statistical Analysis.** For the biomechanical test, six rabbits were used (n=6). Regard to each
39
40 of the histological and micro-CT analysis, three rabbits were used (n=3). The student analysis of
41
42 variance was used to calculate the statistical significance of difference by IBM SPSS statistical
43
44 software package. The p values < 0.05 were considered statistically significant difference.
45
46
47
48
49

50 ASSOCIATED CONTENT

51
52
53 **Supporting Information.** The Supporting Information is available free of charge on the
54
55 ACS Publications website. EDS analysis of R-Ti at the gouge area (Figure S1), SEM
56
57
58
59
60

1
2
3
4 morphology of the R-Ti-TiO₂-SnO₂ (Figure S2), weight of the modified Ti implants with
5
6 different surface structure (Figure S3), Raman spectra of Ti-TiO₂ and Ti-TiO₂-SnO₂ (Figure S4),
7
8 EDS analysis of the pushed-out Ti-TiO₂-SnO₂ in cortical bone region (Figure S5), X-ray
9
10 radiographs of the tibia with placed implants (Figure S6), and schematic diagram for the
11
12 histological morphometry of the VG stained sections (Figure S7); sample code based on the
13
14 structure of implants (Table S1), and comparison of push-out test results of the Ti implant
15
16 fabricated by different modified strategies (Table S2) have been used as supporting information
17
18
19
20
21
22 in this work.
23
24
25
26

27 **AUTHOR INFORMATION**

28 **Corresponding Author**

29
30
31
32 * Yong Han. E-mail: yonghan@xjtu.edu.cn
33

34
35 * Bo Su. E-mail: b.su@bristol.ac.uk
36
37
38
39

40 **Notes**

41
42
43 The authors declare that there is no conflict of interest.
44
45
46
47

48 **ACKNOWLEDGMENT**

49
50
51 The authors gratefully acknowledge the financial support by the State Key Program of
52
53 National Natural Science Foundation of China (Grant No. 51631007), National Natural Science
54
55 Foundation of China (Grant No. 51602251), China Postdoctoral Science Foundation (Grant No.
56
57
58
59
60

1
2
3
4 2016M590941 and 2017T100745), and Fundamental Research Funds for the Central Universities
5
6 (Grant No. xjj2017052). Rui Zhou also gratefully acknowledge the financial support for his
7
8 research visit at the University of Bristol from the China Scholarship Council (Grant No.
9
10 201706285046).
11
12
13

14 15 16 **REFERENCES**

- 17
18 (1) Chen, Q. Z.; Thouas, G. A. Metallic Implant Biomaterials. *Mater. Sci. Eng., R* **2015**, *87*,1–57.
19
20 (2) Stefflik, D. E.; Corpe, R. S.; Young, T. R.; Sisk, A. L.; Parr, G. R. The Biologic Tissue
21
22 Responses to Uncoated and Coated Implanted Biomaterials. *Adv. Dent. Res.* **1999**, *13*, 27–33.
23
24 (3) Fujibayashi, S.; Neo, M.; Kim, H. M.; Kokubo, T.; Nakamura, T. Osteoinduction of Porous
25
26 Bioactive Titanium Metal. *Biomaterials* **2004**, *25*, 443–450.
27
28 (4) Nasab, M. B.; Hassan, M. R.; Sahari, B. B. Metallic Biomaterials of Knee and Hip – A
29
30 Review. *Trends Biomater. Artif. Organs* **2010**, *24*, 69–82.
31
32 (5) Mulari, M. T. K.; Qu, Q.; Harkonen, P. L.; Vaananen, H. K. Osteoblast-Like Cells Complete
33
34 Osteoclastic Bone Resorption and Form New Mineralized Bone Matrix in vitro. *Calcif. Tissue*
35
36 *Int.* **2004**, *75*, 253–261.
37
38 (6) Mori, S.; Burr, D. B. Increased Intracortical Remodeling Following Fatigue Damage. *Bone*
39
40 **1993**, *14*, 103–109.
41
42 (7) Smit T. H.; Burger E. H. Is BMU-Coupling a Strain-Regulated Phenomenon? A Finite
43
44 Element Analysis. *J. Bone Miner. Res.* **2000**, *15*, 301–307.
45
46 (8) Thiel A.; Reumann M. K.; Boskey A.; Wischmann J.; Eisenhart-Rothe R.; Mayer-Kuckuk P.
47
48
49
50
51
52
53
54
55
56
57
58
59
60

1
2
3
4 Osteoblast Migration in Vertebrate Bone. *Biol. Rev.* **2017**, *93*, 350–363.

5
6 (9) Wu, S. L.; Liu, X. M.; Yeung, K. W. K.; Liu, C. S.; Yang, X. J. Biomimetic Porous Scaffolds
7
8 for Bone Tissue Engineering. *Mater. Sci. Eng., R* **2014**, *80*, 1–36.

9
10 (10) Liu, X.; Wu, S.; Yeung, K. W.; Chan, Y. L.; Hu, T.; Xu, Z. S.; Liu, X. Y.; Chung, J. C. Y.;
11
12 Cheung, K. M. C.; Chu, P. K. Relationship between Osseointegration and Superelastic
13
14 Biomechanics in Porous NiTi Scaffolds. *Biomaterials* **2011**, *32*, 330–338.

15
16 (11) Zhou, R.; Wei, D. Q.; Feng, W.; Cheng, S.; Yang, H. Y.; Li, B. Q.; Wang, Y. M.; Jia, D. C.;
17
18 Zhou, Y. Bioactive Coating with Hierarchical Double Porous Structure on Titanium Surface
19
20 Formed by Two-Step Microarc Oxidation Treatment. *Surf. Coat. Technol.* **2014**, *252*, 148–156.

21
22 (12) Yan, Y. Y.; Sun, J. F.; Han, Y.; Li, D. C.; Cui, K. Microstructure and Bioactivity of Ca, P and
23
24 Sr Doped TiO₂ Coating Formed on Porous Titanium by Micro-Arc Oxidation. *Surf. Coat.*
25
26 *Technol.* **2010**, *205*, 1702–1713.

27
28 (13) Yerokhin, A. L.; Nie, X.; Leyland, A.; Matthews, A.; Dowey, S. J. Plasma Electrolysis for
29
30 Surface Engineering. *Surf. Coat. Technol.* **1999**, *122*, 73–93.

31
32 (14) Bai, Y. X.; Zhou, R.; Cao, J. Y.; Wei, D. Q.; Du, Q.; Li, B. Q.; Wang, Y. M.; Jia, D. C.; Zhou
33
34 Y. Microarc Oxidation Coating Covered Ti Implants with Micro-Scale Gouges Formed by A
35
36 Multi-Step Treatment for Improving Osseointegration. *Mater. Sci. Eng., C* **2017**, *76*, 908–917.

37
38 (15) Girard, P. P.; Cavalcanti-Adam, E. A.; Kemkemer, R.; Spatz, J. P. Cellular
39
40 Chemomechanics at Interfaces: Sensing, Integration and Response. *Soft Mater.* **2007**, *3*,
41
42 307–326.

43
44 (16) Ryan, G.; Pandit, A.; Apatsidis, D. P. Fabrication Methods of Porous Metals for Use in
45
46
47
48
49
50
51
52
53
54
55

1
2
3
4 Orthopaedic Applications. *Biomaterials* **2006**, *27*, 2651–2670.

5
6 (17) Sjostrom, T.; McNamara, L. E.; Meek, R. M. D.; Dalby, M. J.; Su, B. 2D and 3D
7
8 Nanopatterning of Titanium for Enhancing Osteoinduction of Stem Cells at Implant Surfaces.
9
10
11 *Adv. Healthcare Mater.* **2013**, *2*, 1285–1293.

12
13 (18) Zhou, J. H.; Li, B.; Lu, S. M.; Zhang, L.; Han, Y. Regulation of Osteoblast Proliferation and
14
15
16 Differentiation by Interrod Spacing of Sr-HA Nanorods on Microporous Titania Coatings. *ACS*
17
18
19 *Appl. Mater. Interfaces* **2013**, *5*, 5358–5365.

20
21 (19) Nepal, M.; Li, L.; Bae, T. S.; Kim, B.; Soh, Y. Evaluation of Osseointegration around Tibial
22
23
24
25
26
27
28
29 Implants in Rats by Ibandronate-Treated Nanotubular Ti-32Nb-5Zr Alloy. *Biomol. Ther.* **2014**, *22*,
30
31
32
33
34
35
36
37 563–569.

38 (20) Yan, J.; Sun, J. F.; Chu, P. K.; Han, Y.; Zhang, Y. M. Bone Integration Capability of A Series
39
40
41
42
43
44
45
46
47
48
49
50
51
52 of Strontium-Containing Hydroxyapatite Coatings Formed by Micro-Arc Oxidation. *J. Biomed.*
53
54
55
56
57
58
59
60 *Mater. Res., Part A* **2013**, *101*, 2465–2480.

(21) Rajabi, A. H.; Jaffe, M.; Arinze, T. L. Piezoelectric Materials for Tissue Regeneration: A
Review. *Acta Biomater.* **2015**, *24*, 12–23.

(22) Campetelli, A.; Bonazzi, D.; Minc, N. Electrochemical Regulation of Cell Polarity and the
Cytoskeleton. *Cytoskeleton* **2012**, *69*, 601–612.

(23) Ning, C.; Zhou, L.; Tan, G. Fourth-Generation Biomedical Materials. *Mater. Today* **2015**, *19*,
2–3.

(24) Liao, J.; Zhu, Y.; Zhou, Z.; Chen, J.; Tan, G.; Ning, C.; Mao, C. Reversibly Controlling
Preferential Protein Adsorption on Bone Implants by Using An Applied Weak Potential as A

1
2
3
4 Switch. *Angew. Chem. Int. Edit.* **2014**, *53*, 13068–13072.

5
6 (25) Ning, C.; Yu, P.; Zhu, Y.; Yao, M.; Zhu, X.; Wang, X.; Lin, Z.; Li, W.; Wang, S.; Tan, G.;
7
8 Zhang, Y.; Wang, Y.; Mao, C. Built-in Microscale Electrostatic Fields Induced by
9
10 Anatase-Rutile-Phase Transition in Selective Areas Promote Osteogenesis. *NPG Asia Mater.*
11
12 **2016**, *8*, e243.

13
14
15 (26) Pfeifer, V.; Erhart, P.; Li, S.; Rachut, K.; Morasch, J.; Brötz, J.; Reckers, P.; Mayer, T.;
16
17 Rühle, S.; Zaban, A.; Seró, I. M.; Bisquert, J.; Jaegermann, W.; Klein, A. Energy Band
18
19 Alignment between Anatase and Rutile TiO₂. *J. Phys. Chem. Lett.* **2013**, *4*, 4182–4187.

20
21 (27) Scanlon, D. O.; Dunnill, C. W.; Buckeridge, J.; Shevlin, S. A.; Logsdail, A. J.; Woodley, S.
22
23 M.; Catlow, C. R. A.; Powell, M. J.; Palgrave, R. G.; Parkin, I. P.; Watson, G. W.; Keal, T. W.;
24
25 Sherwood, P.; Walsh, A.; Sokol, A. A. Band Alignment of Rutile and Anatase TiO₂. *Nat. Mater.*
26
27 **2013**, *12*, 798–801.

28
29 (28) Mobini, S.; Talts, Ü. L.; Xue, R. K.; Cassidy, N. J.; Cartmell, S. H. Electrical Stimulation
30
31 Changes Human Mesenchymal Stem Cells Orientation and Cytoskeleton Organization. *J.*
32
33 *Biomater. Tissue Eng.* **2017**, *7*, 829–833.

34
35 (29) Marino, A. A.; Becker, R. O. Piezoelectric Effect and Growth Control in Bone. *Nature* **1970**,
36
37 *228*, 473–474.

38
39 (30) Zhou, R.; Han, Y.; Cao, J. Y.; Li, M.; Jin, G. R.; Luo, H. T.; Zhang, L. Z.; Su, B. Electrically
40
41 Bioactive Coating on Ti with Bi-layered SnO₂-TiO₂ Hetero-Structure for Improving
42
43 Osseointegration. *J. Mater. Chem. B* **2018**, *6*, 3989–3998.

44
45 (31) Zhou, R.; Wei, D. Q.; Cao, J. Y.; Feng, W.; Cheng, S.; Du, Q.; Li, B. Q.; Wang, Y. M.; Jia, D.

1
2
3
4 C.; Zhou, Y. Conformal Coating Containing Ca, P, Si and Na with Double-Level Porous Surface
5
6 Structure on Titanium Formed by A Three-Step Microarc Oxidation. *RSC Adv.* **2015**,
7
8 5, 28908–28920.

9
10
11 (32) Liang, P.; Liao, C.; Chueh, C.; Zuo, F.; Williams, S. T.; Xin, X.; Lin, J.; Jen, A. K. Y.
12
13 Additive Enhanced Crystallization of Solution-Processed Perovskite for Highly Efficient
14
15 Planar-Heterojunction Solar Cells. *Adv. Mater.* **2014**, 26, 3748–3754.

16
17
18 (33) Kudo, A.; Miseki, Y. Heterogeneous Photocatalyst Materials for Water Splitting. *Chem. Soc.*
19
20 *Rev.* **2009**, 38, 253–278.

21
22
23 (34) Li, J. H.; Wang, J. X.; Wang, D. H.; Guo, G. Y.; Yeung, K. W. K.; Zhang, X. L.; Liu, X. Y.
24
25 Band Gap Engineering of Titania Film through Cobalt Regulation for Oxidative Damage of
26
27 Bacterial Respiration and Viability. *ACS Appl. Mater. Interfaces* **2017**, 9, 27475–27490.

28
29
30 (35) Kulbir, K.; Singh, C. V. Amorphous TiO₂ as A Photocatalyst for Hydrogen Production: A
31
32 DFT Study of Structural and Electronic Properties. *Energy Procedia* **2012**, 29, 291–299.

33
34
35 (36) Huang, J.; Liu, Y.; Lu, L.; Li, L. The Photocatalytic Properties of Amorphous TiO₂
36
37 Composite Films Deposited by Magnetron Sputtering. *Res. Chem. Intermed.* **2012**, 38, 487–498.

38
39
40 (37) Sekiya, T.; Ohta, S.; Kamei, S. Hanakawa, M.; Kurita, S. Raman Spectroscopy and Phase
41
42 Transition of Anatase TiO₂ under High Pressure. *J. Phys. Chem. Solids* **2001**, 62, 717–721.

43
44
45 (38) Frank, O.; Zupalova, M.; Laskova, B.; Kurti, J.; Koltai, J.; Kavan, L. Raman Spectra of
46
47 Titanium Dioxide (Anatase, Rutile) with Identified Oxygen Isotopes. *Phys. Chem. Chem. Phys.*
48
49 **2012**, 14, 14567–14572.

50
51
52 (39) Azam, A.; Habib, S. S.; Salah, N. A.; Ahmed, F. Microwave-Assisted Synthesis of SnO₂
53
54
55

1
2
3
4 Nanorods for Oxygen Gas Sensing at Room Temperature. *Int. J. Nanomed.* **2013**, *8*, 3875–3882.

5
6 (40) Tenkyong, T.; Mary, J. S. S.; Praveen, B.; Pugazhendhi, K.; Sharmila, D. J.; Shyla, J. M.;
7
8 Structural Modulation and Band Gap Optimization of Electrochemically Anodized TiO₂
9
10 Nanotubes. *Mater. Sci. Semicond. Process.* **2018**, *83*, 150–158.

11
12 (41) Chen, J. H.; Liu, C.; You, L.; Simmons, C. A. Boning up on Wolff's Law: Mechanical
13
14 Regulation of the Cells that Make and Maintain Bone. *J. Biomech.* **2010**, *43*, 108–118.

15
16 (42) Cox, B. N.; Smith, D. W. On Strain and Stress in Living Cells. *J. Mech. Phys. Solids* **2014**,
17
18 *71*, 239–252.

19
20 (43) Kurata, K.; Uemura, T.; Nemoto, A.; Tateishi, T.; Murakami, T.; Higaki, H.; Miura, H.;
21
22 Iwamoto, Y. Mechanical Strain Effect on Bone Resorbing Activity and Messenger RNA
23
24 Expressions of Marker Enzymes in Isolated Osteoclast Culture. *J. Bone Miner. Res.* **2001**, *16*,
25
26 722–730.

27
28 (44) Harada, S.; Rodan, G. A. Control of Osteoblast Function and Regulation of Bone Mass.
29
30 *Nature* **2003**, *423*, 349–355.

31
32 (45) Martin, R. B. On the Histologic Measurement of Osteonal BMU Activation Frequency.
33
34 *Bone* **1994**, *15*, 547–549.

35
36 (46) Jerez, S.; Camacho, A. Bone Metastasis Modeling Based on the Interactions between the
37
38 BMU and Tumor cells. *J. Comput. Appl. Math.* **2018**, *330*, 866–876.

39
40 (47) Klein, N. J.; Veldhuijzen, J. P.; Strien, M. E.; de Jong, M.; Burger, E. H. Inhibition of
41
42 Osteoclastic Bone Resorption by Mechanical Stimulation in vitro. *Arthritis Rheumatol.* **1990**, *33*,
43
44 66–72.

- 1
2
3
4 (48) Maejima-Ikeda, A.; Aoki, M.; Tsuritani, K.; Kamioka, K.; Hiura, K.; Miyoshi, T.; Hara, H.;
5
6 Takano-Yamamoto, T.; Kumegawa, M. Chick Osteocyte-Derived Protein Inhibits Osteoclastic
7
8 Bone Resorption. *Biochem. J.* **1997**, *322*, 245–250.
9
10
11 (49) Mackie, E. Osteoblasts: Novel Roles in Orchestration of Skeletal Architecture. *Int. J.*
12
13 *Biochem. Cell Biol.* **2003**, *35*, 1301–1305.
14
15
16 (50) Zhou, R.; Wei, D. Q.; Cao, J. Y.; Feng, W.; Cheng, S.; Du, Q.; Li, B. Q.; Wang, Y. M.; Jia, D.
17
18 C.; Zhou, Y. Synergistic Effects of Surface Chemistry and Topologic Structure from Modified
19
20 Microarc Oxidation Coatings on Ti Implants for Improving Osseointegration. *ACS Appl. Mater.*
21
22 *Interfaces* **2015**, *7*, 8932–8941.
23
24
25
26 (51) Gittens, R. A.; McLachlan, T.; Olivares-Navarrete, R.; Cai, Y.; Berner, S.; Tannenbaum, R.;
27
28 Schwartz, Z.; Sandhage, K. H.; Boyan, B. D. The Effects of Combined
29
30 Micron-/Submicron-Scale Surface Roughness and Nanoscale Features on Cell Proliferation and
31
32 Differentiation. *Biomaterials* **2011**, *32*, 3395–3403.
33
34
35
36 (52) Horie, M.; Fujita, K. Chapter Four - Toxicity of Metal Oxides Nanoparticles. *Adv. Mol.*
37
38 *Toxicol.* **2011**, *5*, 145–178.
39
40
41
42 (53) Ventre, M.; Causa, F.; Netti, P. A. Determinants of Cell-Material Crosstalk at the Interface:
43
44 Towards Engineering of Cell Instructive Materials. *J. R. Soc. Interface* **2012**, *9*, 2017–2032.
45
46
47
48 (54) Xia, L.; Zhang, N.; Wang X.; Zhou, Y.; Mao, L.; Liu, J.; Jiang, X.; Zhang, Z.; Chang, J.; Lin,
49
50 K.; Fang, B. The Synergetic Effect of Nano-Structures and Silicon-Substitution on the Properties
51
52 of Hydroxyapatite Scaffolds for Bone Regeneration. *J. Mater. Chem. B* **2016**, *4*, 3313–3323.
53
54
55
56 (55) Fleig, A.; Penner, R. The TRPM Ion Channel Subfamily: Molecular, Biophysical and
57
58
59
60

1
2
3
4 Functional Features. *Trends Pharmacol. Sci.* **2004**, *25*, 633–639.

5
6 (56) Abed, E.; Moreau, R. Importance of Melastatin-Like Transient Receptor Potential 7 and
7
8 Cations (Magnesium, Calcium) in Human Osteoblast-Like Cell Proliferation. *Cell Proliferation*
9
10
11 **2007**, *40*, 849–865.

12
13 (57) Cheng, H.; Feng, J. M.; Figueiredo, M. L.; Zhang, H.; Nelson, P. L.; Marigo, V.; Beck, A.
14
15
16 Transient Receptor Potential Melastatin Type 7 Channel Is Critical for the Survival of Bone
17
18 Marrow Derived Mesenchymal Stem Cells. *Stem Cells Dev.* **2010**, *19*, 1393–1403.

19
20 (58) Abed, E.; Martineau, C.; Moreau, R. Role of Melastatin Transient Receptor Potential 7
21
22 Channels in the Osteoblastic Differentiation of Murine MC3T3 Cells. *Calcif. Tissue Int.* **2011**, *88*,
23
24
25
26
27 246–253.

28
29 (59) Couchourel, D.; Aubry, I.; Delalandre, A.; Lavigne, M.; Martel-Pelletier, J.; Pelletier, J. P.;
30
31
32 Lajeunesse, D. Altered Mineralization of Human Osteoarthritic Osteoblasts Is Attributable to
33
34 Abnormal Type I Collagen Production. *Arthritis Rheumatol.* **2009**, *60*, 1438–1450.

35
36 (60) Fan, X.; Feng, B.; Liu, Z.; Tan, J.; Zhi, W.; Lu, X.; Wang, J.; Weng, J. Fabrication of TiO₂
37
38
39
40 Nanotubes on Porous Titanium Scaffold and Biocompatibility Evaluation in vitro and in vivo. *J.*
41
42
43 *Biomed. Mater. Res., Part A* **2012**, *100A*, 3422–3427.

44
45 (61) Peng, Wei.; Xu, L.; You, J.; Fang, L.; Zhang, Q. Selective Laser Melting of Titanium Alloy
46
47
48 Enables Osseointegration of Porous Multi-Rooted Implants in A Rabbit Model. *BioMed. Eng.*
49
50
51 *Online.* **2016**, *15*, 85.

52
53 (62) Wang, Q.; Qiao, Y.; Cheng, M.; Jiang, G.; He, G.; Chen, Y.; Zhang, X.; Liu, X. Tantalum
54
55
56 Implanted Entangled Porous Titanium Promotes Surface Osseointegration and Bone Ingrowth.
57
58

1
2
3
4 *Sci. Rep.* **2016**, *6*, 26248.
5

6 (63) Zhou, R.; Wei, D. Q.; Cheng, S.; Feng, W.; Du, Q.; Yang, H. Y.; Li, B. Q.; Wang, Y. M.; Jia,
7 D. C.; Zhou, Y. Structure, MC3T3-E1 Cell Response, and Osseointegration of Macroporous
8 Titanium Implants Covered by A Bioactive Microarc Oxidation Coating with Microporous
9 Structure. *ACS Appl. Mater. Interfaces* **2014**, *6*, 4797–4811.
10
11
12
13
14
15
16
17
18
19
20
21
22
23
24
25
26
27
28
29
30
31
32
33
34
35
36
37
38
39
40
41
42
43
44
45
46
47
48
49
50
51
52
53
54
55
56
57
58
59
60

Table of Contents

